© IWA Publishing 2020
877

Water Practice & Technology Vol 15 No 4
doi: 10.2166/wpt.2020.069

Triple activation (thermal-chemical-physical) in the development of an activated carbon from tobacco: characterizations and optimal conditions for Cd^{2+} and Pb^{2+} removal from waters

Jéssica Manfrin[a,*], Affonso Celso Gonçalves Jr[b], Daniel Schwantes[c], César Ricardo Teixeira Tarley[d], Andréia da Paz Schiller[a] and Gabriel José Klassen[e]

[a] Master of Science in Agronomy, Universidade Estadual do Oeste do Paraná (UNIOESTE), Pernambuco Street, 1777 – Centro, Marechal Cândido Rondon, State of Paraná, Brazil

[b] Universidade Estadual do Oeste do Paraná (UNIOESTE), Pesquisador Produtividade em Pesquisa do CNPq. Pernambuco Street, 1777 - Centro, Marechal Cândido Rondon, State of Paraná, Brazil

[c] Departamento de Ciencias Vegetales, Facultad de Agronomía e Ing, Forestal, Pontificia Universidad Católica de Chile, Avenida Vicuña Mackenna 4860, Macul, Región Metropolitana, Santiago, Chile

[d] Universidade Estadual de Londrina (UEL), Pesquisador Produtividade em Pesquisa do CNPq, Rodovia Celso Garcia Cid – PR 445, Km 380- Campus Universitário, Londrina, State of Paraná, Brazil

[e] Agronomist Engineer, Universidade Estadual do Oeste do Paraná (UNIOESTE), Pernambuco Street, 1777 – Centro, Marechal Cândido Rondon, State of Paraná, Brazil

*Corresponding author. E-mail: jessicamanfrinn@gmail.com

Abstract

This research aimed to transform tobacco that originated from smuggled cigarettes into activated carbons, and to study its application in the remediation of water contaminated by cadmium and lead. For this, a triple activation was performed (thermal – chemical H_3PO_4 – physical CO_2), resulting in the studied activated carbon (CT $H_3PO_4 + CO_2$). The carbon was characterized by its chemical composition, pH_{PZC}, Scanning Electron Microscopy (SEM), FT-IR, Brunauer-Emmett-Teller (BET), and BJH. The influence of the pH of Cd^{2+} and Pb^{2+} solutions, and the influence of the adsorbent dose, were studied. Isotherms were constructed by linear and nonlinear models of Langmuir, Freundlich, Sips, Dubinin-Radushkevich, and Temkin. CT $H_3PO_4 + CO_2$ has carbonates, hydroxyls, carboxylic, and carbonic acids as surface functional groups. The triple activation caused changes in pH_{PZC} (from 5.40 to 9.59). The SEM revealed a carbon surface full of irregular and heterogeneous structures, spongy aspect, with an estimated Specific Surface Area (SSA) increase of 395x and pore volume of 37x. The produced activated carbon has applicability over a wide pH range (3.00–7.00), with an ideal dose estimated at 4 g L^{-1} for greater efficiency in removing Cd^{2+} and Pb^{2}. The linear and nonlinear models reveal that metal adsorption is predominantly physical and multi-layered, with a possible reuse in new sorption cycles.

Key words: alternative adsorbents, biosorbents, cigarettes, decontamination of water, sustainable technology, water treatment

Highlights

- Triple activation was performed (thermal – chemical H_3PO_4 – physical CO_2), resulting in the CT $H_3PO_4 + CO_2$ activated carbon;
- CT $H_3PO_4 + CO_2$ activated carbon has on its surface carbonates, hydroxyls, carboxylic, and carbonic acids, which contribute to the adsorption process;
- Activation increased the Specific Surface Area 395 times and pore volume 37 times;
- CT $H_3PO_4 + CO_2$ activated carbon has applicability over a wide pH range (3.00–7.00), with an ideal dose of 4 g L^{-1} for greater efficiency in removing Cd^{2+} and Pb^{2+}.

Water Practice & Technology Vol 15 No 4
doi: 10.2166/wpt.2020.069

INTRODUCTION

The quality of water matrix is a notorious subject, which has been discussed internationally in recent years, especially due to the dependence of different human activities on this precious resource (Schiller *et al.* 2018). Sustainable Development has been discussed since 1992, in the Rio' 92 UN Conference on Environment and Development. From that conference, many others have been conducted at different periods and locations to discuss problems and try to find solutions, including the water quality concerns (De Santis & Bortone 2018). In this sense, in 2015, the United Nations (UN) launched the 2030 Agenda, which established, among the 17 Sustainable Development Goals (SDGs), the guarantee of safe drinking water and sanitation (UN 2015).

Among the main anthropogenic activities that impact on water resources, we highlight those related to the industrial and agricultural sector (Schiller *et al.* 2019). Among the substances released by these activities, which negatively impact water resources, the most important are toxic metals. These metals can negatively affect the integrity of human health, and cause damage to the environment as a whole (Mahmood & Malik 2014). Moreover, these substances can be bioaccumulated by organisms; that is, they have the ability to persist in different environmental compartments (Tural *et al.* 2016).

Due to their high toxicity, cadmium (Cd^{2+}) and lead (Pb^{2+}) are among the metals that cause serious damage to humans and the environment (Bassegio *et al.* 2019; Conradi *et al.* 2019). The human toxicity for Cd and Pb occurs mostly by contact with inorganic compounds released from sources such as gasoline, paints and ceramic products, batteries, pigments, plastics and agrochemicals, and many others (May *et al.* 2018; Kubier *et al.* 2019).

Cadmium (Cd) is a heavy metal and one of the most toxic metals, classified as a category I carcinogen by the International Cancer Research Agency (IARC 2018). It is widely distributed in the environment as Cd acetate, sulfate, chloride, oxide, and carbonate as a result of various anthropogenic activities related to the industrial processes of Zn, the nickel-cadmium battery, as well as the combustion of fuels that produce gases and particulate matter, tobacco smoke, use of fertilizers and paint additives (Reyes-Hinojosa *et al.* 2019).

More than 80% of the ingested Cd is estimated to come from cereals, mainly rice and wheat (Gonçalves Jr. *et al.* 2020). The absorption of Cd by the lungs through tobacco smoke is estimated to be between 10 and 50%, compared to 8% obtained from food at the gastrointestinal level (Ganguly *et al.* 2018). Cd can affect health in many different ways, from poisoning and anemia to bone, liver, kidney, and lung disease. Also, it can increase the risk of heart failure due to coronary artery damage, diabetes, and oxidative stress (Huang *et al.* 2019; Reyes-Hinojosa *et al.* 2019).

Lead (Pb) is a highly harmful heavy metal comprising 0.002% of the earth's crust. In addition, Pb is the second most toxic metal after As (Zulfiqar *et al.* 2019). The manufacture of acid batteries, insecticides containing Pb, mining, use of fuel containing Pb, printing, and so on, are the main contaminant sources of Pb (Bassegio *et al.* 2019).

Pb does not degrade once mobilized. As a result, significant health risks persist due to residual lead particles released into the environment decades ago (Gonçalves *et al.* 2014). Pb paint remains a problem due to the deterioration of old buildings and the depletion of lead-based vehicles from decades ago. Approximately 24 million households are estimated to have hazardous levels of Pb-based paint or dust, and low-income households are eight times more likely to be at risk. Pb particles from these sources and others deposit in the soil, resurfacing with rain and construction (Rocha & Trujillo 2019), often contaminating water sources through erosion or incorrect discharge of effluents.

Considering the toxicity of Cd and Pb, the World Health Organization established guideline values for Cd and Pb presence in drinking water, which are 0.003 mg L^{-1} for Cd and 0.01 L^{-1} for Pb. However, the guideline value for Pb is provisional, it is based on the treatment performance and analytical

Water Practice & Technology Vol 15 No 4
doi: 10.2166/wpt.2020.069

achievability (WHO 2011a, 2011b). In addition, different countries in the world have assumed maximum allowed values in drinking water for these contaminants; in Brazil, for example, these values are 0.005 mg L^{-1} for Cd and 0.01 L^{-1} for Pb (Brasil 2011a).

Aiming at the decontamination of waters containing these toxic metals, the adsorption process stands out as an alternative with great potential. The adsorption process can be used to remove high or low concentrations of pollutants, being an attractive technology for treatment and post-treatment systems (Gonçalves *et al.* 2016; Gonçalves Jr. *et al.* 2016).

In this sense, the use of commercial activated carbon demands a complex and costly production process (Schiller *et al.* 2020). Given this, the development of activated carbons using alternative materials and processes that result in a lower cost and high performance product becomes attractive to industry as well as to scientific research (Barbosa *et al.* 2014). Among the alternative materials that can be used is tobacco from the seizure of smuggled cigarettes in the western region of the state of Paraná – Brazil (Conradi *et al.* 2019).

The number of cigarettes seized is large and continues to grow each year (Nobrega 2019; Agência Brasil 2018), and its usual disposal is the incineration of the material (Conradi *et al.* 2019). However, if this disposal does not follow the appropriate and environmentally friendly parameters, it may cause environmental damage, such as soil contamination and air pollution. The disposal of this waste is not environmentally appropriate, creating environmental problems on both sides of the Brazil-Paraguay border (Observatory of the National Policy on Tobacco Control 2020). It is important to mention that in cigarettes are found more than 16 PAHs (polycyclic aromatic hydrocarbons), such as naphthalene, acenaphthene, acenaphthene, fluorene, pyrene, chrysene, and so on, in addition to pesticides and toxic metal residues from the agricultural tobacco period (Conradi *et al.* 2019). When these materials are disposed of in the environment, these contaminants quickly leak into the environment (Torkashvand *et al.* 2020). As described above, innovative technological attempts to transform cigarettes and their waste, or to give them a new and correct destination, are sorely needed, especially because these wastes today have improper disposal, causing environmental problems.

The production of an activated carbon can occurs from different activation techniques, including thermal (incomplete pyrolysis), physical (with physical agents such as CO_2 and steam) or chemical (using modifying agents such as $ZnCl_2$, NaOH, H_3PO_4, etc.) (Hokkanen *et al.* 2016). Traditionally, controlled pyrolysis of wood, carbon, and coconut shells produces commercially active carbons (Schiller *et al.* 2020). However, this production usually requires some polymers, all of a certain purity, which may increase the cost of production.

In the production of activated carbon, it is important to note that some characteristics are very desirable, for example, a large surface area and a high mesoporous volume generally determine a good adsorbent product (Conradi *et al.* 2019). These characteristics guarantee to the product an application in different processes, such as separation, discoloration, deodorization, purification, and filtration operations (Xing *et al.* 2019). Also, chemical composition, methods, and process conditions used during the activation, play an important role in the characteristics mentioned before. Consequently, the adsorption properties of activated carbon vary from one source of plant species to another (Reyes-Hinojosa *et al.* 2019).

Thus, the objective of this research was to develop tobacco activated carbons from smuggled cigarettes on the Brazil-Paraguay border using a triple activation process (thermal, physical, and chemical). In addition, this research aims to produce a new and correct destination for these hazardous wastes by generating an environmentally friendly solution by testing these new activated carbons to remove Cd^{2+} and Pb^{2+} from water.

Next, by treating a hazardous toxic waste (cigarette) and turning it into a material to be used in remediation processes such as water treatment facilities and industries, this research highlights a promising and innovative solution to two distinct problems, to mention: the possible cheapening of

Water Practice & Technology Vol 15 No 4
doi: 10.2166/wpt.2020.069

activated carbon production and environmentally sound disposal of smuggled cigarettes on the Brazil-Paraguay border.

MATERIAL AND METHODS

Obtaining of T *in natura* and development of CT $H_3PO_4 + CO_2$

The tobacco used in this study came from the Brazilian Internal Revenue Service (IRS) through seizures in the western region of Paraná, South of Brazil. The tobacco in its fresh form was sent to the Laboratory of Environmental and Instrumental Chemistry of the State University of Western Paraná – UNIOESTE, campus of Marechal Cândido Rondon, for further transformation into activated carbon.

The tobacco was dried in a forced-air oven at 65 °C for a period of 24 h, ground and sieved to standardize particle size on 14 and 65 mesh sieves, obtaining particles between 0.212 and 1.40 mm. For thermal activation, the pyrolysis of the material was performed in a tubular oven (FT 1200 1Z, with internal dimension of 120 × 300 mm, model FE50RPN digital controller). The carbonization occurred only under continuous flow of inert gas N_2 and absence of O_2, until reaching a predetermined temperature of 500 °C for 60 min.

Subsequently, the decanted material was washed with ultrapure water (up to neutral pH) and, subsequently, taken to a lab oven for drying for 4 h at 110 °C (Conradi *et al.* 2019). For chemical activation, 1,000 mL of a 1 mol L^{-1} H_3PO_4 solution was added to the material in the mixing ratio of 10 g of tobacco per 100 mL of solution.

The mixture containing the chemical solution and the material to be activated was kept for 6 h in direct contact and under constant stirring at 45 °C. The resulting material was filtered, washed with ultrapure water and then oven dried for 24 h at 65 °C.

It should be noted that throughout this analytical procedure, the degree of carbonization (burn-off) was determined (Gonçalves *et al.* 2016). As the last step of the activation process, physical activation was conducted. For this, the carbonization occurred only under continuous flow of inert gas N_2 and absence of O_2, until reaching a predetermined temperature of 750 °C. After reaching 750 °C, activation occurred only under continuous flow of CO_2 gas for 60 minutes. All this procedure resulted in the activated carbon named CT $H_3PO_4 + CO_2$.

Characterization of CT $H_3PO_4 + CO_2$ and T *in natura*

Activated carbon CT $H_3PO_4 + CO_2$ (carbon from tobacco chemically activated by H_3PO_4, physically activated by CO_2, and thermal activated at 500 °C) and tobacco sample (T *in natura*) were subjected to chemical characterization by nitroperchloric digestion (AOAC 2012), with subsequent determination of metal concentrations in its composition by FAAS (Welz & Sperling 2008).

In order to study the morphological, chemical, and physical characteristics of CT $H_3PO_4 + CO_2$ and its source material (T *in natura*), both materials were subjected to the following analytical determinations: pH of the point of zero charge (pH_{PZC}) as adapted from Mimura *et al.* (2010), Scanning Electron Microscopy – SEM, Infrared spectrum – FT-IR, BET - Brunauer *et al.* (1938), and BJH - Barrett *et al.* (1951).

Contaminated water samples

To assess the adsorption capacity of the activated carbon in contaminated water, synthetic contamination of the water samples with toxic metals was performed, which were prepared from certified standards diluted in ultrapure water. The solutions were prepared from certified Cd^{2+} standards

Water Practice & Technology Vol 15 No 4
doi: 10.2166/wpt.2020.069

with cadmium nitrate salts ($Cd(NO_3)_2$. $4H_2O$ P.A. ≥99.0% Sigma-Aldrich), and Pb^{2+} with lead nitrate salts ($Pb(NO_3)_2$ P.A. ≥99.0%).

The concentrations studied were defined based on the National Council of Environment – CONAMA resolutions N° 357 of 2005, N°. 430 of 2011 (Brasil 2005, 2011b), and N°. 2,914 of 2011 of the Ministry of Health (Brasil 2004, 2011a), which establish the maximum permitted values of toxic metals and other contaminants in water.

Adsorption studies

In order to investigate the adsorption process, studies were carried out to evaluate the influence of adsorbent dose (CT $H_3PO_4 + CO_2$ and T *in natura*), as well as the influence of medium pH on the removal process of Cd^{2+} and Pb^{2+}.

Thus, from the 1,000 mg L^{-1} mono-elemental solutions, the solutions with the desired concentrations for each study were prepared, buffered to the predetermined pH values, as presented in Table 1, by addition of NaOH and HCl, both at 0.1 mol L^{-1}.

Table 1 | Central matrix of the DCCR planning

Tests	X_1	Mass (mg)	X_2	pH
1	− 1.00	396.39	− 1.00	3.60
2	1.00	1,103.61	− 1.00	3.60
3	− 1.00	396.39	1.00	6.40
4	1.00	1,103.61	1.00	6.40
5	0.00	750.00	0.00	5.00
6	− 1.41	250.00	0.00	5.00
7	0.00	750.00	1.41	7.00
8	1.41	1,250.00	0.00	5.00
9	0.00	750.00	− 1.41	3.00
10	0.00	750.00	0.00	5.00
11	0.00	750.00	0.00	5.00
12	0.00	750.00	0.00	5.00

Note: X_1: codification for the variable mass. X_2: codifications for the variable pH. Based on the study of Conradi *et al.* (2019).

Using a Central Rotational Compound Design (CRCD) (Barros Bruns & Scarminio 2010), the doses of adsorbents in the range of 5–25 g L^{-1} (250–1,250 mg in each 125 mL reactor) were evaluated, with pH variations within the range from 3.00 to 7.00 (Table 1).

To this end, 50 mL of the mono-elemental solution containing Cd^{2+} or Pb^{2+} in 125 mL conical flasks was added, with the modified adsorbent masses, which were then placed in a thermostated Dubnoff system with constant stirring at 200 rpm for 1.5 hours at 25 °C.

After the assortment process in the Dubnoff system, the samples were filtered and aliquots were taken to determine the final metal concentrations by FAAS (Welz & Sperling 2008). From the obtained values for equilibrium concentration, the amount adsorbed at equilibrium was calculated (Equation (1)).

$$q_e = \frac{(C_o - C_{e)} \times V}{m} \quad (1)$$

Water Practice & Technology Vol 15 No 4
doi: 10.2166/wpt.2020.069

In equation (1), q_e is the amount of adsorbed ion per g of adsorbent in equilibrium (mg g^{-1}), m is the used mass of adsorbent (g), C_0 is the initial ion concentration (mg L^{-1}), C_e is the concentration of ion in equilibrium (mg L^{-1}) and V is the used volume of solution (L).

The obtained results from the aforementioned tests were tabulated and evaluated according to multivariate analysis with the aid of Statistica 5.0 software. The percentage of Cd^{2+} and Pb^{2+} removal was calculated according to Equation (2):

$$\%R = 100 - \left(\frac{C_f}{C_0} \times 100\right) \quad (2)$$

In which % R is the percentage of metal removal by the adsorbent, C_f is the metal final concentration (mg L^{-1}) and C_0 is the initial concentration of metal in the solution (mg L^{-1}).

Adsorption isotherms were also constructed. For this purpose, samples of CT $H_3PO_4 + CO_2$ and T *in natura* adsorbents were placed in 125 mL conical flasks, and set in contact with 50 mL of Cd^{2+} and Pb^{2+} solutions. The experimental conditions for this study were: adsorbent dose 4 g L^{-1}, pH of the contaminant solution of 5.00, constant system temperature of 25 °C, and contact time between adsorbent and adsorbate of 90 min. The concentrations of Cd^{2+} and Pb^{2+} evaluated were: 5, 30, 60, 90, 120, 150, 180, 210, 240, 270, and 300 mg L^{-1}. The obtained results were evaluated by the linear and nonlinear models of Langmuir, Freundlich, Dubinin-Radushkevich, Sips, and Temkin.

All the aforementioned experimental routine was performed in triplicate, with certified standards and ultrapure water. Graphs and results of linear and nonlinear models were generated using Origin 8.0 software. The equations employed in this study are exhibited in Table 2.

RESULTS AND DISCUSSION

Degree of materials carbonization and characterizations of the materials

The carbonization degree of CT $H_3PO_4 + CO_2$ obtained was 37.38%. According to Gonçalves *et al.* (2016), the precursor material as well as the activations employed directly influence the material structure and characteristics at the end of the process. Similarly, material profitability, expressed by the burn-off index, is directly related to the precursor material and the established activation method. The same author also mentions that the profitability of activated carbon after carbonization varies on average between 40 and 80%.

Characterization of CT $H_3PO_4 + CO_2$ and T *in natura*

The results in Table 3 show a change in the concentration of chemical elements in CT $H_3PO_4 + CO_2$ when compared to T *in natura* (Conradi *et al.* 2019), a decrease of P (0.84x), K (0.09x), Ca (0.56x), Mg (0.56x), Mn (0.77x) and Pb (0.07x) being observed; whereas Cu (4.70x), Zn (21.42x), and Fe (2.84x) concentrations increase.

Phosphoric acid acts as a cleansing agent and cleans the tars deposited in the biochar pores (Oginni *et al.* 2019), this satisfactorily explains the decrease of P, K, Ca, Mg, Mn and Pb concentration in the CT $H_3PO_4 + CO_2$.

It is noteworthy that among the activating agents, H_3PO_4 is one of the most widely used for the activation of lignocellulosic biomass, because it is less dangerous for the environment, is easily recovered by washing with water, is reusable, produces less corrosion than alkaline hydroxides, and produces high yields (Negara *et al.* 2020). In addition, it is possible to adjust the textural properties and surface chemistry of activated carbon by precisely selecting the conditions used during the activation process with H_3PO_4 (Quesada-Plata *et al.* 2016).

Water Practice & Technology Vol 15 No 4
doi: 10.2166/wpt.2020.069

Table 2 | Mathematical models used for equilibrium studies

Used adsorption models		
Langmuir (Langmuir 1918) (linear)	$\frac{C_e}{q_e} = \frac{1}{q_m b} + \frac{C_e}{q_m}$	C_e (mg L^{-1}): concentration of the metal in the equilibrium; q_e (mg g^{-1}): amount of metal adsorbed in the equilibrium per unit of adsorbent mass; q_{max}: maximum capacity of adsorption (mg g^{-1}); k_L or $q_m b$: adsorbent-adsorbate interaction forces (L mg^{-1}).
(nonlinear)	$q_e = q_{max}\, k_L\, \frac{C_e}{(1 + k_L\, C_e)}$	
Freundlich (Freundlich 1906) (linear)	$\log q_e = \log k_f + \left(\frac{1}{n}\right) \log\ C_e$	C_e (mg L^1): concentration of the metal in the equilibrium; q_e (mg g^1): amount of metal adsorbed in the equilibrium per unit of adsorbent mass; k_f [mg g^{-1} (mg $L^{-1})^{-1/n}$] and n (dimensionless): Freundlich parameters.
(nonlinear)	$q_e = k_f C_e^{\frac{1}{n}}$	
Dubinin-Radushkevich (Dubinin e Radushkevich 1947) (linear)	$\ln q_e = \ln qd \quad - Bd\ \varepsilon^2$ $\varepsilon = RT \ln\ \left(1 + \frac{1}{C_e}\right)$	C_e (mol L^{-1}): concentration of the metal in the equilibrium; q_e (mol g^{-1}): amount of metal adsorbed in the equilibrium per unit of adsorbent mass; q_d (mol L^{-1}): adsorption capacity; q_{max} (mol g^{-1}): maximum capacity of adsorption; B_d (mol^2 J^{-2}): coefficient related to sorption energy; 'ε': Polanyi potential; R: universal gas constant (8.314 J mol^{-1} K^{-1}); T: temperature (K).
(nonlinear)	$q_e = q_{max}\left(\exp\left(-B_d RTLn\left(1 + \frac{1}{C_e}\right)\right)\right)^2$	
Sips (Sips 1948) (linear)	$\ln\left(\frac{q_e}{q_{max} - q_e}\right) = \frac{1}{n} ln C_e + \frac{1}{n} ln k_L$	C_e (mg L^{-1}): concentration of the metal in the equilibrium; q_e (mg g^{-1}): amount of metal adsorbed in the equilibrium per unit of adsorbent mass; q_{max} (mg g^{-1}) maximum capacity of adsorption; n (dimensionless) relates to the heterogeneity of adsorbent material; k_L is the adsorbent-adsorbate interaction forces.
(nonlinear)	$q_e = q_{max}\, k_s C_e^{\left(\frac{n}{1 + k_s C_e^n}\right)}$	
Temkin (Temkin & Pyzhev 1940) (linear)	$q_e = B\, ln A_t + B \ln C_e$	C_e (mg L^{-1}): concentration of the metal in the equilibrium; q_e (mg g^{-1}): amount of metal adsorbed in the equilibrium per unit of adsorbent mass; A_t (L g^{-1}) is the equilibrium binding constant; b_t is the Temkin isotherm constant (dimensionless); R: universal gas constant (8.314 J mol^{-1} K^{-1}); T: temperature at 298 K. B (J mol^{-1}): constant related to the heat of sorption, obtained by the expression $B = RT/b_t$.
(nonlinear)	$q_e = \left(\frac{RT}{b_t}\right) \ln (A_t C_e)$	

Table 3 | Chemical composition of the materials T *in natura* and CT $H_3PO_4 + CO_2$

Adsorbents	P g Kg^{-1}	K	Ca	Mg	Cu	Zn mg kg^{-1}	Mn	Fe	Cd	Pb	Cr
T *in natura*	5.92	44.80	26.10	5.88	10.00	19.00	175.67	283.00	< LQ	26.67	< LQ
CT $H_3PO_4 + CO_2$	4.96	3.85	14.70	3.30	47.00	407.00	136.00	805.00	1.00	2.00	75.00
T *in natura*/activated carbon	**0.84**	**0.09**	**0.56**	**0.56**	**4.70**	**21.42**	**0.77**	**2.84**	–	**0.07**	–

Note: LQ (limits of quantification in mg L^{-1}): K = 0.01, Ca = 0.005, Mg = 0.005, Cu = 0.005, Fe = 0.01, Mn = 0.01, Zn = 0.005, Cd = 0.005, Pb = 0.01, Cr = 0.01 (mg kg^{-1}). Red values indicate the loss of the element concentration comparing to the precursor T *in natura* (by T *in natura*/activated carbon). Blue values indicate the increase of the element concentration comparing to the precursor T *in natura* (by T *in natura*/activated carbon). T *in natura* values described by Conradi *et al.* (2019).

Similar changes in adsorbent composition were also observed by Schwantes *et al.* (2018a), when performing chemical modifications with H_2SO_4, NaOH, and H_2O_2 in different vegetable biomass. According to Kan *et al.* (2018) the volatilization of components during material carbonization (thermal activation) is responsible for the loss of volatiles and the increase in the content of various nonvolatile elements such as metals. Then, it can explain the increase in Cu, Zn, and Fe.

Water Practice & Technology Vol 15 No 4
doi: 10.2166/wpt.2020.069

In addition, activating chemical solutions used in the chemical activation step can extract or modify the composition of the final carbon. Another factor to consider, which explains the decrease in element concentration, is the washing of carbon to neutral pH, which possibly removed much of what was once solubilized in the adsorbent (Nacke *et al.* 2017; Schwantes *et al.* 2018b).

The following pH_{PZC} values were obtained: 5.40 for T *in natura* (Conradi *et al.* 2019) and 9.59 for CT $H_3PO_4 + CO_2$ (Figure 1). According to Schwantes *et al.* (2018b), the adsorbent, upon contact with the liquid solution with pH lower than pH_{PZC}, will have its surface positively charged, suggesting the preference for adsorption of anions by the active sites formed, due to the protonation and deprotonation of groups on the surface materials.

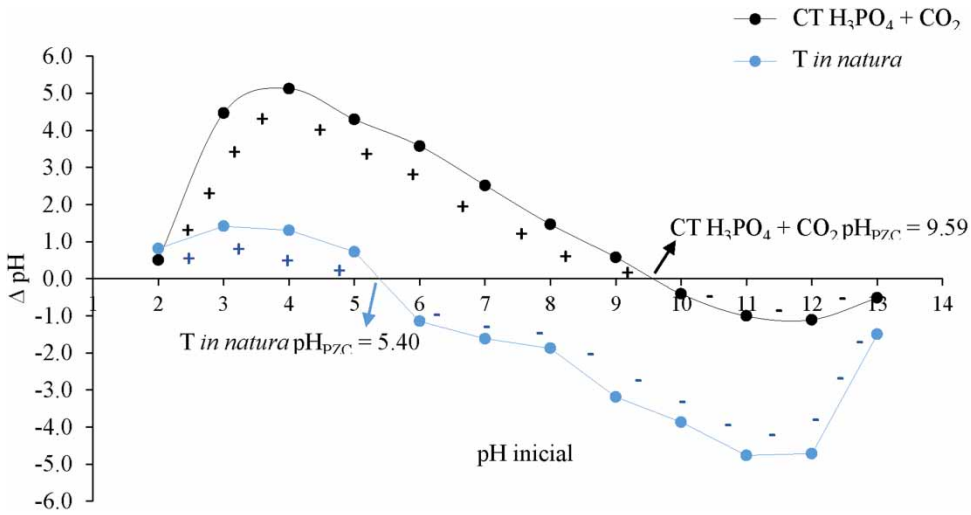

Figure 1 | Graph expressing the pH_{PZC} for the studied adsorbents, exhibiting the predominance of surface + or – charges, depending on the pH of the solution and the pH_{PZC} of the material.

Similarly, in aqueous solutions with a pH higher than pH_{PZC}, the adsorbent surface is negatively charged, preferentially absorbing more cations than anions, a process that can be explained by the electrostatic attraction between the electrical charge generated on the adsorbent surface and the anionic group or cationic solution (Mimura *et al.* 2010; Tagliaferro *et al.* 2011).

Nacke *et al.* (2017) obtained different pH_{PZC} in biosorbents from different structures of *Jatropha curcas* L., Bohli *et al.* (2015); when producing activated carbon from olive stones, obtained pH_{PZC} much lower than those found in the present study. This shows that the great variation of the adsorbent pH_{PZC} may depend on the material source, the process used to obtain the adsorbent, and moreover the types of adopted activations which will characterize the material and may provoke changes in its structure (Conradi *et al.* 2019).

The visualization of the samples obtained by SEM (Figure 2) shows variations in the surface morphology of the adsorbents. T *in natura* has some homogeneity in its surface, whereas the activated carbon CT $H_3PO_4 + CO_2$ exhibited irregular and heterogeneous structures, spongy aspect, reminding to a lesser extent its precursor.

The characteristics observed in tobacco adsorbents are very similar to those observed by Nacke *et al.* (2017) and Schwantes *et al.* (2018a) in biosorbents from *Jatropha curcas* L. and cassava and pine bark. According to Nacke *et al.* (2017) and Conradi *et al.* (2019), characteristics such heterogeneity and spongy aspect may indicate good adsorption capacity.

It can be inferred from Table 4 that the FT-IR spectra observed in Figure 3 show that the main functional groups capable of acting on the adsorption of Cd^{2+} and Pb^{2+} are hydroxyl, carbonyl, carboxylic, amine, and carbonate.

Water Practice & Technology Vol 15 No 4
doi: 10.2166/wpt.2020.069

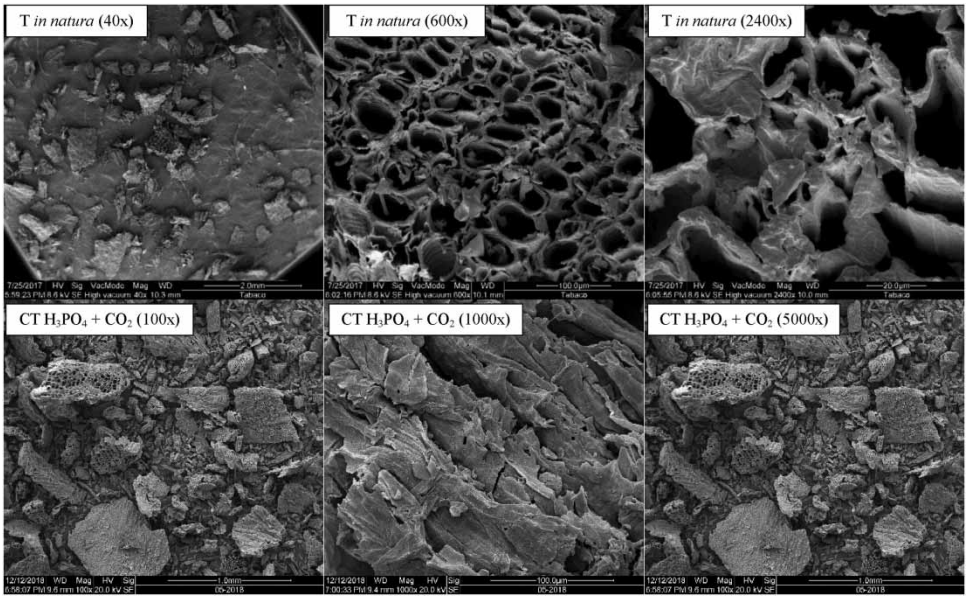

Figure 2 | Scanning Electron Microscopy (SEM) for the materials T *in natura* (Conradi *et al.* 2019) in approximations of 40, 600, and 2.400 times. For CT $H_3PO_4 + CO_2$ in approximations of 100, 1.000, and 5.000 times.

Table 4 | Summary of selected groups in the infrared spectrum in the region between 722 and 3,449 cm

Wavelength (cm^{-1})	Vibration	Functional group
3,449–3,382	O-H	Bonded and unbound hydroxyl groups and water [a,b]
2,361–2,356	C = O	Different isotopic CO_2 molecules formed in reactions[a,c]
1,623	C-C	Nucleic acids (carbonyl and carboxyl groups)[d]
1,445–1,400	C-H	Lipids (fatty acids), polysaccharides (pectin), and preoteins[e]
1,057–1,038	C-O	Functional groups present in lignin (amines and hydroxyls)[a,f]
874–722	C-O	Carbonate[f,g]

Source: [a]Silverstein *et al.* (2014). [b]Feng *et al.* (2011). [c]Conradi *et al.* (2019). [d]Onorevoli *et al.* (2018). [e]Peng & Wu (2010). [f]Chen *et al.* (2017).

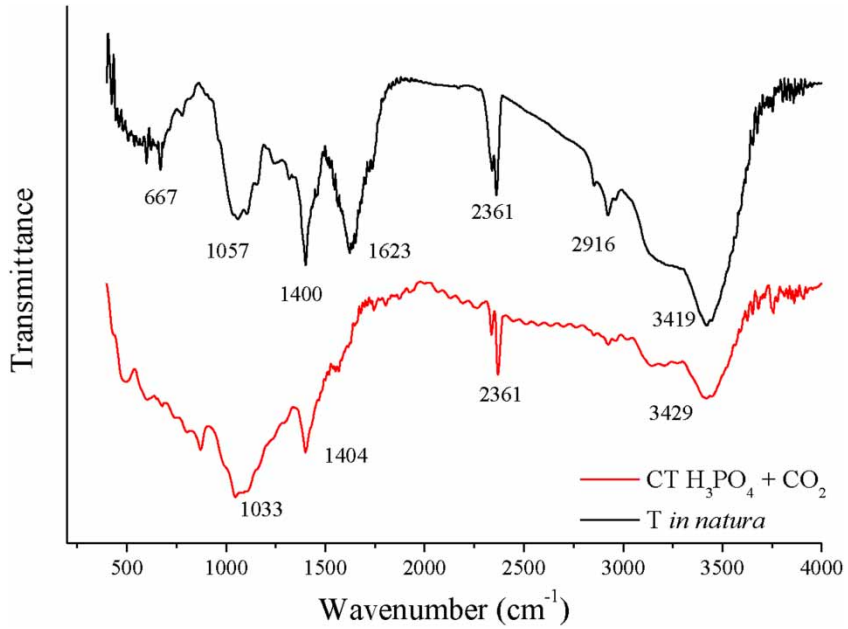

Figure 3 | Infrared spectrum analysis from 4,000 a 400 nm^{-1} for T *in natura* and CT $H_3PO_4 + CO_2$.

Water Practice & Technology Vol 15 No 4
doi: 10.2166/wpt.2020.069

The wave lengths found near 3,400 cm^{-1} suggest the presence of O-H stretch vibrations due to the presence of water (Feng *et al.* 2011; Silverstein *et al.* 2014). The bands with values between 2,361 and 2,356, found for adsorbents T *in natura* and CT $H_3PO_4 + CO_2$, indicate vibrational stretching C = O; suggesting the presence of different isotopic molecules of CO_2 formed in reactions (Silverstein *et al.* 2014; Conradi *et al.* 2019).

In T *in natura* it is possible to observe C-C vibrational stretching, with the presence of bands at 1,623 cm^{-1}, which can be attributed to the presence of carbonyl and carboxyl functional groups (Onorevoli *et al.* 2018). For CT $H_3PO_4 + CO_2$ bands from 1,445 to 1,400 cm^{-1} were found, suggesting the presence of C-H vibrational strains, possibly due to the presence of lipids, polysaccharides, and proteins (Peng & Wu 2010).

The bands between 1,038 and 1,057 cm^{-1}, referring to the C-O vibrational stretches, can be attributed to the presence of hydroxyls, and amines in the source material. Such a characteristic is of great importance as it may favor the interaction between the metal ion and the adsorbent surface (Silverstein *et al.* 2014; Chen *et al.* 2017).

The wavelengths between 874 cm^{-1} and 722 cm^{-1} show the presence of CO, suggesting carbonates in CT $H_3PO_4 + CO_2$. It is a very positive aspect, since this group can act on retention of metal ions (He *et al.* 2015; Chen *et al.* 2017).

When comparing the infrared spectra of T *in natura* and CT $H_3PO_4 + CO_2$, many of the groups are repeated, demonstrating that the modified material retains characteristics of its precursor, except for the formation of carbonates, exclusively in CT $H_3PO_4 + CO_2$.

Table 5 shows that the surface area found for T *in natura* (0.27 $m^2\ g^{-1}$) is similar to other *in natura* adsorbents present in the literature, as found by Penha *et al.* (2016) 1.13 $m^2\ g^{-1}$ in rice husk and by Oliveira & Franca (2011) 0.46 $m^2\ g^{-1}$ in rice bran. However, a 395-fold increase in surface area for CT $H_3PO_4 + CO_2$ was observed, as well as a 37-fold increase in pore volume.

Table 5 | Specific surface area (SSA), pore volume, and pore diameter for tobacco adsorbents

	Parameters		
Materials	**SSA ($m^2\ g^{-1}$)**	**Pore volume ($cm^3\ g^{-1}$)**	**Pore diameter (nm)**
T *in natura*	0.27	0.0008	2.18
CT $H_3PO_4 + CO_2$	106.80	0.0296	1.68
Relation [activated carbon/T *in natura*]	**395.56**	**37.00**	**0.77**

Note: Red values indicate the decrease of the parameters comparing to the precursor T *in natura* (by activated carbon/T *in natura*); Blue values indicate the increase of the parameter comparing to the precursor T *in natura* (by activated carbon/T *in natura*). T *in natura* values described by Conradi *et al.* (2019).

Ibrahim *et al.* (2016) obtained similar values to those found for CT $ZnCl_2$ when producing activated carbon produced from the aquatic plant *Ulva lactuca* (345.40 $m^2\ g^{-1}$).

It is worth noting that these values are lower when compared to the values obtained for commercial activated carbon (894.00 $m^2\ g^{-1}$) (Merk®). Bohli *et al.* (2015) found SSA in activated carbon from olive pits higher than commercial carbon, reaching 1,194 $m^2\ g^{-1}$, demonstrating that the use of alternative materials in the production of activated carbon can be extremely promising in the development of new adsorbent materials.

Adsorbent T *in natura* (0.0008 $cm^3\ g^{-1}$) presented pore volume similar to that observed by Penha *et al.* (2016) in rice husks (0.0019 $cm^3\ g^{-1}$) and Schwantes *et al.* (2018a) in NaOH modified cassava bark (0.0015 $cm^3\ g^{-1}$).

CT $H_3PO_4 + CO_2$ has lower pore volume than those found by Ibrahim *et al.* (2016), which obtained values of 0.320 $cm^3\ g^{-1}$ for *Ulva lactuva* activated carbon and 0.108 $cm^3\ g^{-1}$ for *Ulva lactuca* biosorbent.

Water Practice & Technology Vol 15 No 4
doi: 10.2166/wpt.2020.069

It is important to mention that the pore diameter of precursor material and CT $H_3PO_4 + CO_2$ is larger than several other adsorbents of plant origin. Schwantes *et al.* (2018a) obtained, in a study with biosorbent of cassava peels modified with H_2O_2, a diameter of 1.73 nm and for NaOH modified shells of diameter 1.92 nm. Moreover, Ibrahim *et al.* (2016) found a pore volume of 1.11 nm and 1.85 nm for *Ulva lactuva* as biosorbent and activated carbon, respectively.

Thus, the results of porous structure analysis of the samples presented in Table 5 indicate that the activation process caused a decrease in pore diameter and, in general, an increase in SSA and pore volume. However, the intraparticle adsorption process of Cd^{2+} and Pb^{2+} may be hampered by reducing the pore diameter too much, since the estimated ionic radius of Cd^{2+} is 0.95 nm and Pb^{2+} is 0.118 nm (Marcus 1993).

The results show that both the precursor material and activated carbon present predominantly microporous texture, since the pore diameter found is smaller or very close to 2.00 nm (IUPAC 1985), being one of the main characteristics that favor the adsorption process (Kawahigashi 2012).

In addition, CT $H_3PO_4 + CO_2$ exhibits Type I isotherm (Figure 4), whose pores are typically micropores, with the exposed surface residing almost exclusively within the micropores, which once occupied, leave little or no external surface for later adsorption (Shamsudin *et al.* 2019).

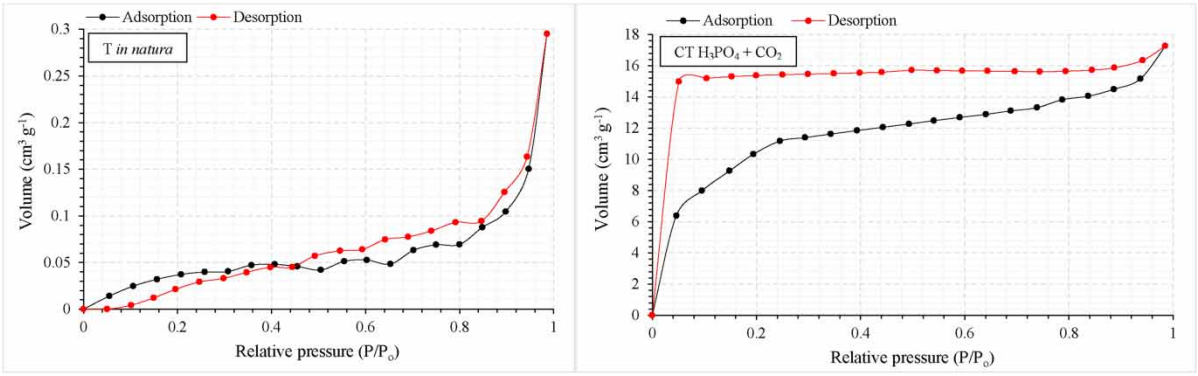

Figure 4 | BET adsorption and desorption isotherms for T *in natura* and CT $H_3PO_4 + CO_2$. T *in natura* values described by Conradi *et al.* (2019).

T *in natura* exhibits a type II isotherm (sigmoid isotherm) characteristic of low porosity systems. These are most often found when adsorption occurs on non-porous powders or diameters larger than micropores. The tipping point occurs near the completion of the first adsorbed monolayer (Thommes *et al.* 2015).

As noted in the above results, changes in adsorbent materials are evident, including increased porosity and specific surface area (Table 5), loss or gain of functional groups originally present in tobacco biomass (Figure 3 and Table 4), besides modifications in the structural morphology of CT $H_3PO_4 + CO_2$ (Figure 2), which may influence the removal rate of organic and inorganic contaminants in aqueous solutions.

Adsorption studies

As can be observed in Table 6, a statistical difference at a 5% level of significance for the adsorbent doses was found, showing that the metal adsorption (Pb or Cd) depends closely on the adsorbent dose, not depending on the studied pH range (3.0–7; 0).

Figure 5 shows the response surfaces for the removal of Cd^{2+} and Pb^{2+} by increasing adsorbent doses *versus* the influence of the solution pH. The highest removal capacity of Cd^{2+} and Pb^{2+} was observed with the smallest amount of available material (4 g L^{-1}). This is a very positive result, since it is evident that even in dosages considered low, the removal is significantly high.

Water Practice & Technology Vol 15 No 4
doi: 10.2166/wpt.2020.069

Table 6 | ANOVA of the predicted model for the influence of adsorbent doses and solution pH on the removal of Cd^{2+} and Pb^{2+} from contaminated waters

		Cd^{2+}		Pb^{2+}	
CV	**DF**	**T *in natura***	**CT $H_3PO_4 + CO_2$**	**T *in natura***	**CT $H_3PO_4 + CO_2$**
Dose (L)	1	10,658.71**	11,500.39**	9,041.788**	3,160.528**
Dose (Q)	1	2,141.89**	2,442.39**	1,491.599**	514.707**
pH (L)	1	0.03	49.43	1.910	169.297
pH (Q)	1	5.31	17.55	0.137	91.999
Dose x pH	1	0.00	40.75	6.625	4.803
Error	6	51.61	56.72	21.352	28.511
Total	11				

Note: CV, coefficient of variation. DF, degrees of freedom. ** Statistically significant at 1% of probability.

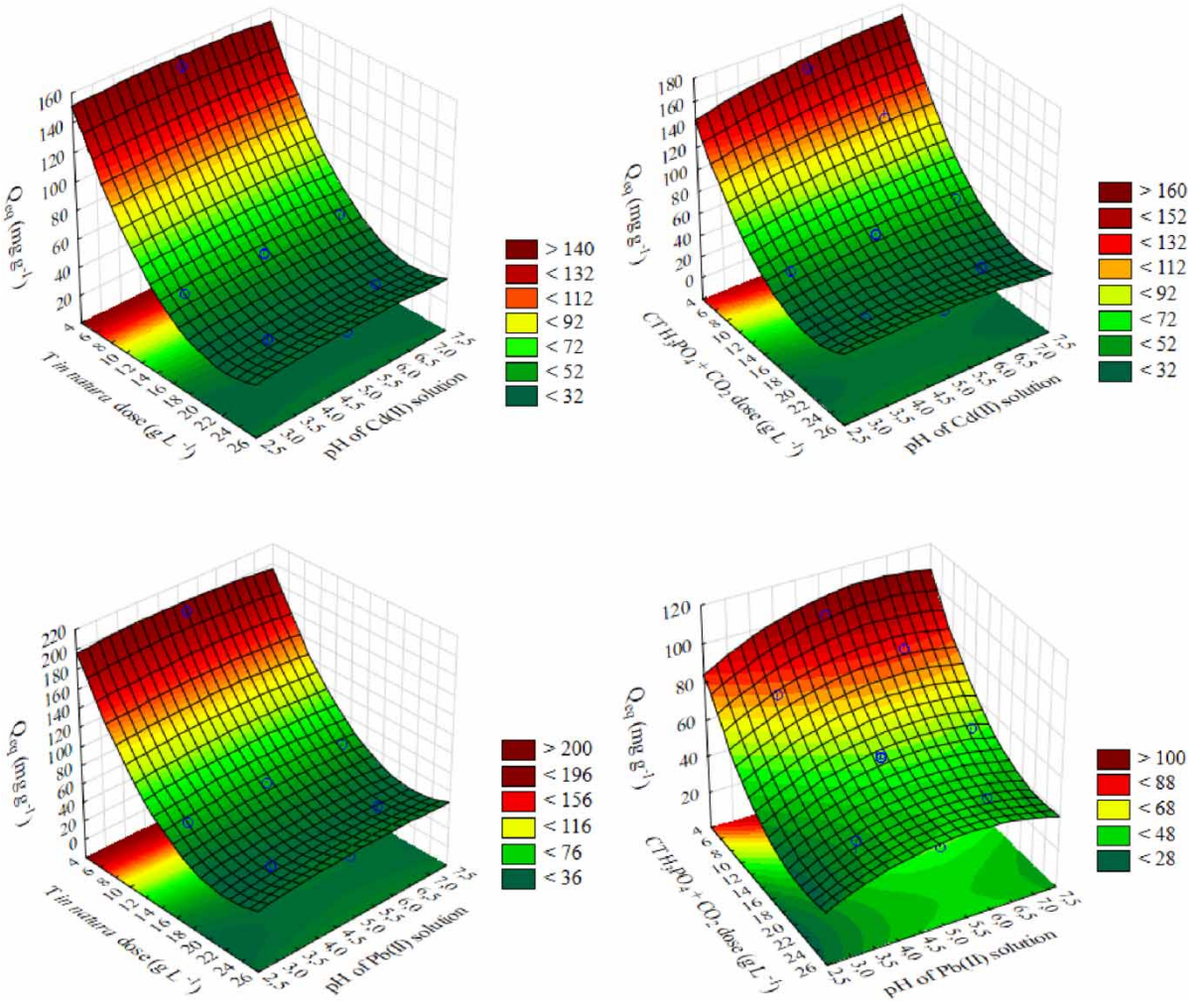

Figure 5 | Response surfaces for Cd^{2+} and Pb^{2+} removal as a function of adsorbing dose and pH effect of contaminant solution. Experimental conditions: 1.5 h stirring; 200 rpm at 25 °C; Masses of 200–1,400 mg in 50 mL, i.e. 4 g L^{-1}–28 g^{-1}. [T *in natura*; Cd^{2+}] $z = 201.36116 - 16.15196x + 0.36622x^2 + 4.52439y - 0.45775y^2 + 0.00071xy$; Adj-$R^2 = 0.976$ [T *in natura*; Pb^{2+}] $z = 259.81646 - 21.93129x + 0.49680x^2 + 8.25111y - 0.86341y^2 + 0.04926xy$; Adj-$R^2 = 0.949$ [CT $H_3PO_4 + CO_2$; Cd^{2+}] $z = 170.79405 - 15.48180x + 0.39107x^2 + 14.92367y - 0.83215y^2 - 0.32237xy$; Adj-$R^2 = 0.976$ [CT $H_3PO_4 + CO_2$; Pb^{2+}] $z = 64.80010 - 7.64316x + 0.17952x^2 + 23.98017y - 1.90509y^2 - 0.11066xy$; Adj-$R^2 = 0.959$.

Water Practice & Technology Vol 15 No 4
doi: 10.2166/wpt.2020.069

It is noteworthy that, in certain cases, it is possible to observe the decrease of the contaminant removal capacity, due to the increase of the adsorbent availability, since the formation of agglomerates in the material can reduce the total surface area and therefore the number of active sites available for the process (El-Sadaawy & Abdelwahab 2014).

Another important aspect is the variation of the maximum adsorption capacity (q_e) observed for each adsorbent, a fact that enhances the diversity of interactions between adsorbent and adsorbate, and its influence on contaminant removal potential (Rodriguez *et al.* 2018).

Excellent mathematical adjustments were obtained for the Langmuir linear model for CT $H_3PO_4 + CO_2$; that is, this model represents the experimental data with high reliability due to the low values of σ (standard deviation) and high values for R^2. This suggests the occurrence of adsorption on monolayers of Cd^{2+} and Pb^{2+} by CT $H_3PO_4 + CO_2$.

Good mathematical adjustments were also obtained for the nonlinear Langmuir model, showing once again the occurrence of Cd^{2+} monolayers for T *in natura*, and CT $H_3PO_4 + CO_2$, as well as Pb^{2+} monolayers observed for T *in natura*. When comparing these two cases, there is a great similarity of the linear and nonlinear estimation results, especially for CT $H_3PO_4 + CO_2$ in the removal of Cd^{2+}, and T *in natura* in the removal of Pb^{2+}.

Estimated q_m values for T *in natura* are higher when removing Cd^{2+} (q_m T *in natura* = 135.1 mg g^{-1}) and Pb^{2+} (q_m T *in natura* = 56.8 mg g^{-1}) when compared to the activated carbon, suggesting that for T *in natura*, adsorption preference occurs in monolayers. According to Araújo *et al.* (2018), Langmuir's model states that all sites are equivalent and each site can contain at most one adsorbate molecule, the sorting process being dependent on chemical affinity; that is, through chemical bonds between the adsorbent and adsorbate. This may be indicative of the low reuse capacity of T *in natura* biosorbents in the removal of Cd^{2+} and Pb^{2+}.

Moreover, the more regular surface of T *in natura*, as observed in Figure 2, corroborates the hypothesis that the adsorption sites are more homogeneous for this natural adsorbent. This also agrees with the results obtained by Langmuir, which show the occurrence of chemical interactions between adsorbent-adsorbate and sorption in monolayers.

The k_f values obtained by the linear modeling show that CT $H_3PO_4 + CO_2$ has high Cd^{2+} adsorption capacity in multilayers (k_f CT $H_3PO_4 + CO_2$ = 3.2 mg g^{-1}), which also suggests a possible predominance of physical interactions between adsorbent- adsorbate at many sites, which may be a good indication of reuse of carbons activated in more than one adsorption cycle.

This result may characterize that carbon activated by H_3PO_4 and CO_2, interact with Cd^{2+} and Pb^{2+} in solution through physical forces, such as Van der Waals, enabling the process of material desorption and reuse (Conradi *et al.* 2019).

For the estimation of k_f by nonlinear models, good adjustments were found only for Cd^{2+} adsorption by CT $H_3PO_4 + CO_2$. In this case, the values of 1/n are between 0 and 0.7, which is evident in highly curved isotherms, as observed for the case cited, in Figure 6.

For linear modeling of D-R, the E obtained values (sorption energy) for CT $H_3PO_4 + CO_2$ in Cd^{2+} adsorption suggest the predominance of a chemical process that governs sorption, since in this case $E > 8$ KJ mol^{-1}. Similarly, adsorption of Cd^{2+} by T *in natura* and for biosorbent, and carbon in Pb^{2+} sorption, $E < 8$ KJ mol^{-1} is observed, suggesting physical sorption.

In contrast, when using the nonlinear Dubinin-Radushkevich model, E values slightly higher than 8 KJ mol^{-1} are observed, suggesting that the adsorption of Cd^{2+} and Pb^{2+} by natural adsorbents and activated carbon of tobacco is of a chemical nature.

As described by Králik (2014), chemical adsorption has the following characteristics: it is similar to a chemical bond, with high heat of adsorption (20–400 kJ mol^{-1}), with the formation of a surface compound (monolayer). Thus, this process is irreversible because 'desorbed compounds' are different from adsorbed compounds; it has high activation energy (similar to a chemical reaction) and high specificity of adsorbent-adsorbate interactions.

Water Practice & Technology Vol 15 No 4
doi: 10.2166/wpt.2020.069

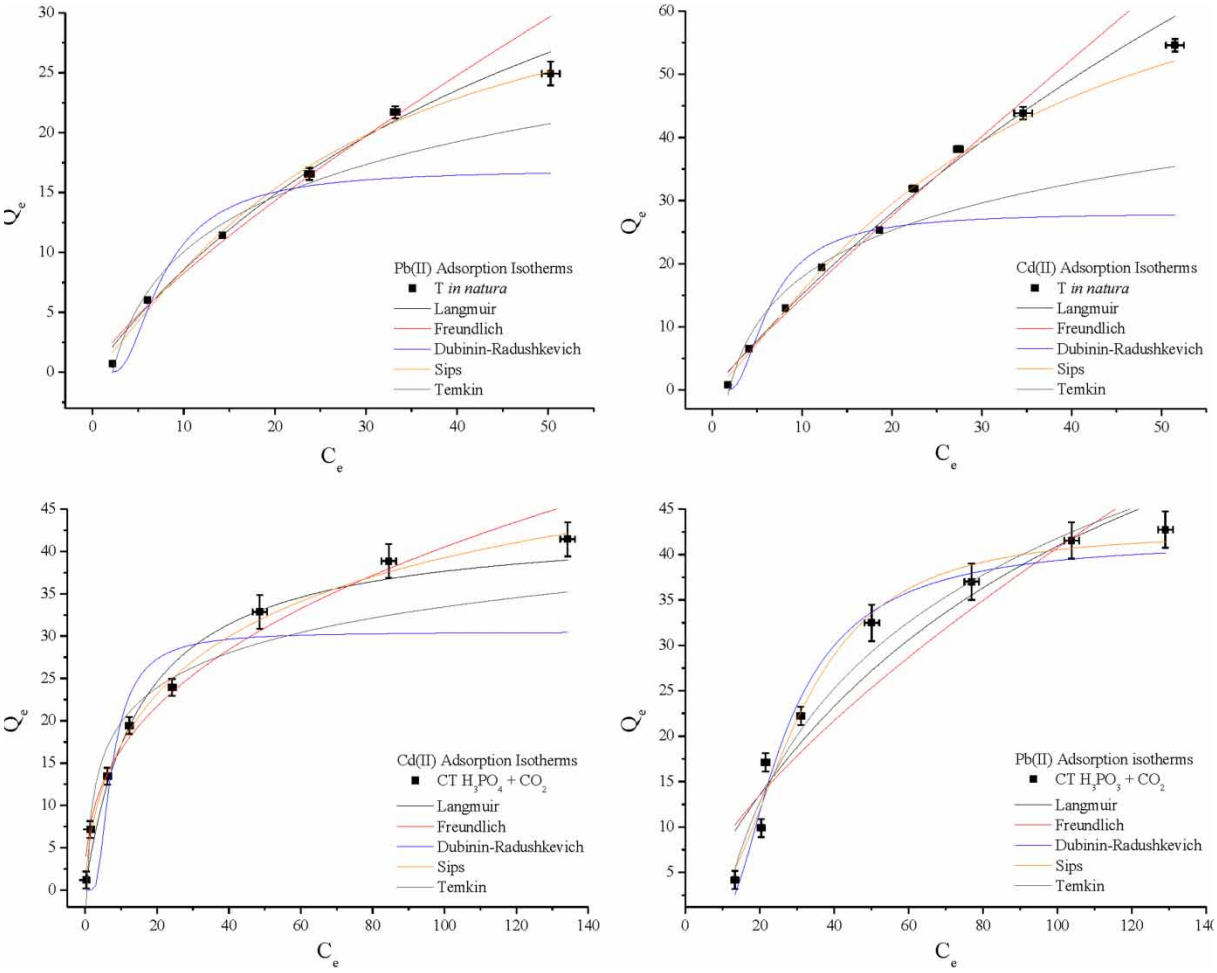

Figure 6 | Nonlinear isotherms of adsorption for T *in natura* and CT $H_3PO_4 + CO_2$ in the removal of Cd^{2+} and Pb^{2+}.

According to Nethaji *et al.* (2013), when Sips parameter ns assumes values <1, the isotherm assumes a rectangular shape; if $n_s > 2$, the isotherm reaches equilibrium (q_{max}) at a lower metal concentration; when $n_s = 1$, the Sips isotherm takes the form of the Langmuir isotherm, showing predominant adsorption in monolayers.

According to Table 7, regarding the use of linear model of Sips, $n_s = 1$ values are observed for Pb^{2+} adsorption by T *in natura*, suggesting the occurrence of a surface with more homogeneous active sites, which corroborates the homogeneity observed in Figure 2 for this biosorbent, as well as results already evidenced by the Langmuir model.

For the non-linear Sips model, n_s values ≈ 1 for T *in natura* are observed in Cd^{2+} and Pb^{2+} adsorption, again suggesting that in these cases the Sips model indicates the preference for adsorption in monolayers. Also noteworthy, the n_s values >2 (for Pb^{2+} adsorption) by nonlinear Sips model for CT $H_3PO_4 + CO_2$, suggesting rapid saturation of surface sites (Özer *et al.* 2016).

Overall, as observed in the micrographs of Figure 2, CT $H_3PO_4 + CO_2$ has high heterogeneity. Due to these heterogeneous morphological and physiological characteristics, there is a possibility that there is more than one type of adsorption site interacting with the contaminant, and thus adsorption may occur in both mono and multilayers. This fact may be related to the morphological variation of the materials and the different characteristics of surface area, pore volume, and pore diameter, which can also be confirmed by the results obtained by Sips, which for CT $H_3PO_4 + CO_2$ suggests the occurrence of adsorption of Cd^{2+} and Pb^{2+} in mono and multilayers.

Water Practice & Technology Vol 15 No 4
doi: 10.2166/wpt.2020.069

Table 7 | Linear and nonlinear parameters of adsorption for Langmuir, Freundlich, D-R, Sips, and Temkin models for the removal of Cd^{2+} and Pb^{2+}

	Cd^{2+}				Pb^{2+}			
Models	**T *in natura***	**σ**	**CT $H_3PO_4 + CO_2$**	**σ**	**T *in natura***	**σ**	**CT $H_3PO_4 + CO_2$**	**σ**
Langmuir (linear) $\frac{1}{q_e} = \frac{1}{C_m} + \frac{1}{k_L C_m C_e}$ and $R_L = \frac{1}{(1 + C_0 K)}$ with two C_0 values (5 and 300 mg L^{-1})								
q_m (mg g^{-1})	135.135	$6.21e^{-4}$	44.444	$6.72e^{-4}$	56.818	0.001	44.053	0.152
k_L (L mg^{-1})	0.014	0.018	0.084	$3.99e^{-2}$	0.018	0.043	0.110	0.002
R_L	0.311–0.964		0.129–0.899		0.159–0.919		0.128–0.898	
$Adj\text{-}R^2$	0.973		0.995		0.923		0.984	
Freundlich (linear) $\log q_{eq} = \log k_f + \left(\frac{1}{n}\right) \log C_e$								
k_f [mg g^{-1} $(mgL^{-1})^{-1/n}$]	1.834	0.038	3.266	0.046	1.480	0.046	0.002	0.541
n	1.089	0.031	1,460	0.035	1.303	0.030	0.375	0.413
$Adj\text{-}R^2$	0.993		0.995		0.991		0.913	
D-R (linear) $\ln q_e = \ln q_d - B d\varepsilon^2$ and $\varepsilon = RT\ln\left(1 + \frac{1}{C_e}\right)$ and $E = \frac{1}{\sqrt{2B_d}}$								
q_d (mol L^{-1})	0.010	0.127	0.001	0.049	0.009	0.175	$1.00e^{-4}$	0.344
B_d	0.008	$2.74e^{-4}$	0.004	$9.90e^{-5}$	0.009	$3.66e^{-4}$	0.009	6.077
E (KJ mol^{-1})	7.857		11.785		7.180		7.454	
$Adj\text{-}R^2$	0.998		0.996		0.990		0.314	
Sips (linear) $q_{eq} = \frac{q_{max}(k_s C_e)^n}{1 + (k_s C_e)^n}$								
n_s	0.582	0.071	1.238	0.034	1.033	0.042	0.338	0.955
k_s (L mg^{-1})	0.017	0.21	0.048	0.108	0.018	0.139	0.026	0.317
$Adj\text{-}R^2$	0.974		0.990		0.961		0.919	
Temkin (linear) $q_{eq} = B\, lnA_t + B \ln C_e$								
A_t (L mg^{-1})	0.488		0.815		0.225		0.815	
b_t	46.960	3.627	113.400	1.057	22.063	10.613	113.400	2.693
B (J mol^{-1})	52.759	4.906	21.848	1.057	112.294	19.258	21.848	1.656
$Adj\text{-}R^2$	0.977		0.991		0.974		0.991	
Langmuir (nonlinear) $q_e = q_m\, k_L \frac{C_e}{(1 + k_L C_e)}$ and $R_L = \frac{1}{(1 + C_0 k)}$ with two C_0 values (5 and 300 mg L^{-1})								
q_m (mg g^{-1})	200.278	101.367	45.861	2.346	56.980	17.602	82.892	24.219
k_L (L mg^{-1})	0.008	0.005	0.057	0.010	0.017	0.007	0.010	0.004
R_L	0.294–0.962		0.05–0.78		0.160–0.919		0.26–0.95	
$Adj\text{-}R^2$	0.974		0.980		0.974		0.884	
Freundlich (nonlinear) $q_e = k_f C_e^{\frac{1}{n}}$								
k_f [mg g^{-1} $(mgL^{-1})^{-1/n}$]	1.727	3.290	7.249	0.938	1.323	0.369	1.716	0.802
n	1.081	0.078	2.707	0.227	1.259	0.147	1.454	0.241
$Adj\text{-}R^2$	0.963		0.977		0.953		0.838	
D-R (nonlinear) $q_e = q_{max}(\exp\left(-B_d RTLn\left(1 + \frac{1}{C_{eq}}\right)\right)^2$ and $\varepsilon = RT\ln\left(1 + \frac{1}{C_e}\right)$ and $E = \frac{1}{\sqrt{2B_d}}$								
q_{max} (mol L^{-1})	0.007	0.001	0.001	$7.51\ e^{-5}$	0.002	$4.91e^{-4}$	0.002	$7.08\ e^{-4}$
B_d	0.007	$3.63e^{-4}$	0.004	$1.97\ e^{-4}$	0.006	$6.36e^{-4}$	0.006	$9.61\ e^{-4}$
E (KJ mol^{-1})	8.265		11.801		9.098		9.098	
$Adj\text{-}R^2$	0.991		0.991		0.977		0.977	

(*Continued.*)

Water Practice & Technology Vol 15 No 4
doi: 10.2166/wpt.2020.069

Table 7 | Continued

Models	Cd^{2+}				Pb^{2+}			
	T *in natura*	σ	CT $H_3PO_4 + CO_2$	σ	T *in natura*	σ	CT $H_3PO_4 + CO_2$	σ
Sips (nonlinear) $q_e = q_{sat} k_s C_e^{\left(\frac{n}{1+k_s C_e^n}\right)}$								
q_{max}	77.806	22.607	62.275	8.506	35.914	12.843	45.512	3.479
n_s	1.275	0.145	0.653	0.075	1.240	0.264	2.459	0.533
k_s ($L\ mg^{-1}$)	0.013	0.003	0.085	0.009	0.018	0.006	2.44 e^{-4}	3.96 e^{-4}
$Adj\text{-}R^2$	0.983		0.994		0.974		0.956	
Temkin (nonlinear) $q_e = \left(\frac{RT}{b_t}\right) \ln(A_t C_e)$								
A_t ($L\ mg^{-1}$)	0.529	0.066	2.317	0.877	0.453	0.066	0.101	0.010
b_t	231.384	26.271	368.077	36.141	373.068	38.168	136.992	11.685
B ($J\ mol^{-1}$)	10.708		6.731		6.641		18.085	
$Adj\text{-}R^2$	0.901		0.937		0.950		0.952	

Note: q_{max}: maximum adsorption capacity, k_L: constant related to adsorbent/adsorbate interaction forces, adj-R^2: adjusted determination coefficient, k_f: related to adsorption capacity, n: related to solid heterogeneity, q_d: maximum adsorption capacity, E: average sorption energy, ε: potential of Polanyi; B_d: coefficient related to sorption energy (Dubinin-Radushkevich); k_s: is the Sips constant. A_t: Temkin isotherm equilibrium binding constant; b_t: Temkin isotherm constant; B: Constant related to heat of sorption; σ: standard deviation. Equilibrium time = 45 minutes; pH of the contaminant solutions = 5.0.

The b_t values <0 for linear and nonlinear Temkin corroborate that the process of adsorption of Cd^{2+} and Pb^{2+} by T *in natura* and CT $H_3PO_4 + CO_2$ is exothermic (Pongener *et al.* 2018). In addition, B (sorption heat) values ranged from 6.73 to 112.29 J mol^{-1}, demonstrating that the adsorbent-adsorbate interaction occurs by physical adsorption; that is, with values below 20 KJ mol^{-1}.

According to Temkin, the heat of surface adsorption of ions decreases linearly and not logarithmically with the coating. Furthermore, according to this model, adsorption is characterized by a uniform distribution of binding energies on the adsorbent surface, encompassing interactions between adsorbent-adsorbent (Nascimento *et al.* 2014).

For chemical adsorption to occur, the heat of adsorption must be of the order of the heat of reaction; that is, above 20 Kcal mol^{-1} (Nascimento *et al.* 2014). In this sense, Temkin's B values (linear and nonlinear) are in the order of 1.60 cal mol^{-1}–26.8 cal mol^{-1}, which is far below, suggesting the predominance of physical forces in the sorption of Cd^{2+} and Pb^{2+}, such as Van der Waals forces, and other intermolecular forces (Conradi *et al.* 2019).

When comparing the developed adsorbents (T *in natura* and CT $H_3PO_4 + CO_2$) with results from the literature (Table 8), superiority in the removal of Cd^{2+} and Pb^{2+} is observed. T *in natura* obtained 135.13 mg g^{-1} in Cd^{2+} removal, considerable value when compared to other biosorbents, such as *Ulva lactuva* (62.50 mg g^{-1}) (Ibrahim *et al.* 2016) and *Jatropha curcas* (229.66 mg g^{-1}) (Nacke *et al.* 2017).

However, the tobacco material in its fresh form (*in natura*) presents high toxicity and toxic elements in its composition. Torkashvand *et al.* (2020) mentions that there are more than 16 PAHs (polycyclic aromatic hydrocarbons) such as naphthalene, acenaphthylene, acenaphthene, fluorene, pyrene, chrysene, etc. In addition to pesticides and toxic metals, residues from the tobacco growing period are found in the cigarette after burning; when they are disposed of in the environment, there is a rapid leakage of these contaminants into the environment (Conradi *et al.* 2019).

Moreover, when this material is subjected to pyrolysis and activation processes resulting in activated carbon, most of the aforementioned toxic materials are volatilized during the process, ensuring that the final material has a very small amount of toxic compounds (CHEN *et al.* 2014), which even in residual amounts are unavailable and insolubilized in the carbonaceous matrix. This

Water Practice & Technology Vol 15 No 4
doi: 10.2166/wpt.2020.069

Table 8 | Comparison of Cd^{2+} and Pb^{2+} removal capacity for T in natura and CT H_3PO_4 to other adsorbent materials cited in the literature

Adsorbent	q_m (mg g^{-1}) Cd^{2+}	Reference	Adsorbent	q_m (mg g^{-1}) Pb^{2+}	Reference
Olive stone (CA)	11.72	Alslaibi *et al.* (2014)	*Ulva lactuca* (CA)	83.30	Ibrahim *et al.* (2016)
Bamboo (CA)	0.19	Lo *et al.* (2012)	Bamboo (CA)	0.67	Lo *et al.* (2012)
Ulva Lactuca (CA)	84.60	Ibrahim *et al.* (2016)	Olive stone (CA)	147.52	Bohli *et al.* (2015)
Grape residues (CA)	58.20	Sardella *et al.* (2015)	Cattle bones (CA)	32.10	Lo *et al.* (2012)
Mangosteen stone (Biosorbent)	3.15	Zein *et al.* (2010)	*Ulva lactuca* (Biosorbent)	68.90	Ibrahim *et al.* (2016)
Ulva lactuca (Biosorbent)	62.50	Ibrahim *et al.* (2016)	*Jatropha Curcas* L. (Biosorbent)	22.90	Nacke *et al.* (2017)
Barks of *Jatropha Curcas* L. (Biosorbent)	29.66	Nacke *et al.* (2017)	Barks of cassava (Biosorbent)	42.46	Schwantes *et al.* (2018a)
Barks of pine (Biosorbent)	10.83	Schwantes *et al.* (2018b)	Activated tobacco by $ZnCl_2$ (CA)	84.75	Conradi *et al.* (2019)
T *in natura* (Biosorbent)	135.13	This research	T *in natura* (Biosorbent)	56.81	This research
CT $H_3PO_4 + CO_2$ (CA)	44.44	This research	CT $H_3PO_4 + CO_2$ (CA)	44.05	This research

Note: CA means activated carbon.

findings were also confirmed by Conradi *et al.* (2019), performing similar chemical activations on tobacco materials. The aforementioned authors state that this procedure (triple activation on tobacco wastes) is extremely attractive for the production of activated carbon, which can be used to treat water and effluents, contaminated especially with toxic metals such as Cd^{2+} and Pb^{2+}.

Estimates and the Brazilian scenario

According to the estimates from the Brazilian Institute of Public Opinion and Statistics (Ibope), described by a report from Nobrega (2019) and exhibited in Figure 7, in 2019 about 76,080 metric tonnes of illegal tobacco in the Brazilian territory were commercialized, and according to our estimates, and if all that smuggled tobacco amount was seized, could be used to produce 30,432 metric tonnes of activated carbon (AC) that could be used in the decontamination of 7,608,000 m^3 of water. Thus, considering a water consumption of 200 L $hab^{-1}day^{-1}$, this could mean that the produced amount of tobacco AC could be used for water treatment systems, during one year successfully removing pollutants and supplying water for a city of about 104,219 inhabitants.

CONCLUSION

The use of chemical activation with H_3PO_4, with subsequent carbonization at 750 °C, in addition to the physical activation with CO_2 for activated carbon production, caused significant changes in tobacco, evidencing functional surface groups such as carbonates, hydroxyls, carboxylic, and carbonic acids (FT-IR). Also, this method of production showed a significant change in pH_{PZC} (from 5.40 to 9.59), as well as a decrease in the concentration of most chemical elements (P, K, Ca, Mg, Mn, Pb) in the activated carbon chemical composition.

It is noteworthy that the carbon produced has irregular and heterogeneous structures, a spongy aspect (SEM), with an increase of 395× SSA and 37× pore volume, which makes it extremely attractive for use as a commercial adsorbent material.

Water Practice & Technology Vol 15 No 4
doi: 10.2166/wpt.2020.069

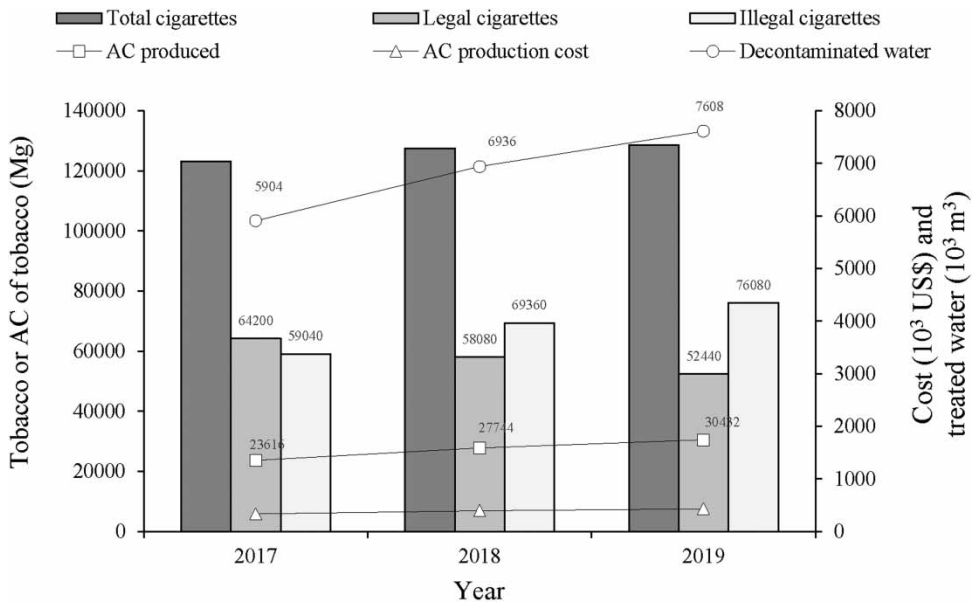

Figure 7 | Predicted legal and illegal tobacco sales in Brazil during 2017–2019 (Nobrega 2019, based on IBOPE data), and estimative of activated carbon (AC) production and cost. Note: considering 1 US$ = R$ 5.33; experimental oven of power = 4,000 W; 120 minutes for the production of 18 g of AC with an average yield of 40%; KWh price (based on São Paulo prices in 2020) = 0.16 US$; 10% of the cost is due to reagent and operational expenses; estimate cost to produce 1 Kg of AC = 78 US$. The estimates presented in Figure 7 were obtained by the experimental laboratory conditions of this research. Estimates that consider industrial conditions (oven, pyrolysis, reagents, etc.) could be 10 or 100 times cheaper.

Furthermore, activated carbon modified with H_3PO_4 and CO_2 has applicability over a wide pH range (3.00–7.00), the ideal carbon dose being 4 g L^{-1}, the recommended dose for an efficient removal of Cd^{2+} and Pb^{2+} from solutions.

The good experimental adjustments obtained for the linear and nonlinear models of Langmuir, Freundlich, Dubinin-Radushkevich, Sips, and Temkin demonstrate that, despite the heterogeneous structure, Cd^{2+} and Pb^{2+} adsorption by carbons is predominantly physical and multilayer, apart from some exceptions, where there is predominance of chemical affinity and adsorption in monolayers, such as is found in the precursor material T *in natura*.

ACKNOWLEDGEMENTS

This study was financed in part by the Coordenação de Aperfeiçoamento de Pessoal de Nível Superior – Brasil (CAPES) – Finance Code 001.

DATA AVAILABILITY STATEMENT

All relevant data are included in the paper or its Supplementary Information.

REFERENCES

AGÊNCIA BRASIL 2018 *Comércio ilegal de cigarros supera mercado regular no Brasil*. Available from: http://agenciabrasil.ebc.com.br/economia/noticia/2018-11/comercio-ilegal-de-cigarros-supera-mercado-regular-no-brasil (accessed 26 October 2019).

Alslaibi, T. M., Abustan, I., Ahmad, M. A. & Foul, A. A. 2014 Preparation of activated carbon from olive stone waste: optimization study on the removal of Cu^{2+}, Cd^{2+}, Ni^{2+}, Pb^{2+}, Fe^{2+}, and Zn^{2+} from aqueous solution using response surface methodology. *Journal of Dispersion Science and Technology* **35**. doi:10.1080/01932691.2013.809506.

Water Practice & Technology Vol 15 No 4
doi: 10.2166/wpt.2020.069

AOAC. Association of Official Analytical Chemist. 2012 *Official Methods of Analysis of the Association Analytical Chemists*, 19th edn. AOAC, Maryland.

Araújo, C. S. T., Almeida, I. L. S., Rezende, H. C., Marcionilio, S. M. L. O., Léon, J. J. L. & Matos, T. N. 2018 Elucidation of mechanism involved in adsorption of Pb(II) onto lobeira fruit (*Solanum lycocarpum*) using Langmuir, Freundlich and Temkin isotherms. *Microchemical Journal* **137**, 348–354. doi:10.1016/j.microc.2017.11.009.

Barbosa, C. S., Santana, S. A. A., Bezerra, C. W. B. & Silva, H. A. S. 2014 Remoção de compostos fenólicos de soluções aquosas utilizando carvão ativado preparado a partir do aguapé (*Eichhornia crassipes*): estudo cinético e de equilíbrio termodinâmico. *Química Nova* **37**(3), 447–453. doi:10.5935/0100-4042.20140066.

Barret, E. P., Joyner, L. G. & Halenda, P. P. 1951 The determination of pore volume and area distributions in porous substances. Computation from nitrogen isotherms. *Journal of American Chemistry Society* **73**, 373–380. doi:10.1021/ja01145a126.

Barros, N. B., Bruns, R. E. & Scarminio, I. S. 2010 *How do Experiments: Applications in Science and Industry*, 4th edn. Bookman, New York, NY.

Bassegio, C., Campagnolo, M. A., Schwantes, D., Gonçalves, J. R., Manfrin, J., Schiller, A. d. P. & Bassegio, D. 2019 Growth and accumulation of Pb by roots and shoots of *Brassica juncea* L. *International Journal of Phytoremediation* **22**(13), 134–139. doi:10.1080/15226514.2019.1647406.

Bohli, T., Ouederni, A., Fiol, N. & Villaescusa, I. 2015 Evaluation of an activated carbon from olive stones used as an adsorbent for heavy metal removal from aqueous phases. *Comptes Rendus Chimie* **18**, 88–99. doi:10.1016/j.crci.2014.05.009.

BRASIL 2004 *Ministério da Saúde*. Portaria n° 518. Brasília, DF, p. 34. Available from: http://bvsms.saude.gov.br/bvs/publicacoes/portaria_518_2004.pdf (accessed 12 September 2019).

BRASIL 2005 *Conselho Nacional do Meio Ambiente (CONAMA)*. Resolução CONAMA n. 357, de 17 de março de 2005. Brasília, DF, p. 27. Available from: http://www2.mma.gov.br/port/conama/legiabre.cfm?codlegi=459. (accessed 12 September 2019).

BRASIL. 2011a *Ministério da Saúde*. Portaria n° 2.914. Brasília, DF, p. 33. Available from: http://bvsms.saude.gov.br/bvs/saudelegis/gm/2011/prt2914_12_12_2011.html (accessed 12 September 2019).

BRASIL 2011b *Conselho Nacional do Meio Ambiente (CONAMA)*. Resolução CONAMA n. 430, de 13 de maio de 2011. Brasília, DF, p. 9. Available from: http://www2.mma.gov.br/port/conama/legiabre.cfm?codlegi=646 (accessed 12 September 2019).

Brunauer, S., Emmett, P. H. & Teller, E. 1938 Adsorption of gases in multimolecular layers. *Journal of American Chemistry Society* **60**, 309–319. https://doi.org/10.1021/ja01269a023.

Chen, H., Li, J., Wu, X., Wang, X. & Wang, X. 2014 Synthesis of alumina-modified cigarette soot carbon as an adsorbent for efficient arsenate removal. *Industrial & Engineering Chemistry Research* **53**, 16051–16060. doi:10.1021/ie503057 g.

Chen, H., Guo, Y. C., Wang, F., Wang, G., Qi, P., Guo, X., Dai, B. & Yu, B. 2017 An activated carbon derived from tobacco waste for use as a supercapacitor electrode material. *New Carbon Materials* **32**(6), 592–599. doi:10.1016/S1872-5805(17)60140-9.

Conradi, J. R., Gonçalves Jr., E., Schwantes, A. C., Manfrin, D., Schiller, J., da P, A., Zimmerman, J., Klassen, G. J. & Ziemer, G. L. 2019 Development of renewable adsorbent from cigarettes for lead removal from water. *Journal of Environmental Chemical Engineering* **7**(4), 103200. doi:10.1016/j.jece.2019.103200.

De Santis, G. & Bortone, C. 2018 International conferences on sustainable development and climate from Rio de Janeiro to Paris. In: *Climate Change and Air Pollution* (Akhtar, R. & Palagiano, C., eds). Springer Climate, New York, NY. https://doi.org/10.1007/978-3-319-61346-8_3.

Dubinin, M. M. & Radushkevich, L. V. 1947 Sorption and structure of active carbons. I. Adsorption of organic vapors. *Zhurnal Fizicheskoi Khimii* **21**(3), 151–162.

El-Sadaawy, M. & Abdelwahab, O. 2014 Adsorptive removal of nickel from aqueous solutions by activated carbons from doum seed (Hyphaenethebaica) coat. *Alexandria Engineering Journal* **53**, 399–408.

Feng, N., Guo, X., Liang, S., Zhu, Y. & Liu, J. 2011 Biosorption of heavy metals from aqueous solutions by chemically modified orange peel. *Journal of Hazardous Materials* **185**, 49–54.

Freundlich, H. M. F. 1906 Over the adsorption in solution. *Journal of Physical Chemistry* **57**, 385–471.

Ganguly, K., Levänen, B., Palmberg, L., Akensson, A. & Lindén, A. 2018 Cadmium in tobacco smokers: a neglected link to lung disease? *European Respiratory Society* **27**(147). doi:10.1183/16000617.0122-2017.

Gonçalves Jr., A. C., Schwantes, D., De Sousa, R. F. B., Da Silva, T. R. B., Guimarães, V. F., Campagnolo, M. A., De Vasconcelos, E. S. & Zimmermann, J. 2020 Phytoremediation capacity, growth and physiological responses of *Crambe abyssinica* Hochst on soil contaminated with Cd and Pb. *Journal of Environmental Management* **262**, 110342. doi:10.1016/j.jenvman.2020.110342.

Gonçalves Jr., A. C., Nacke, H., Schwantes, D. & Coelho, G. F. 2014 Heavy metal contamination in Brazilian Soil due to application of fertilizers. In: *Environmental Risk Assessment of Soil Contamination* (Hernandez Soriano, M. C., ed). IntechOpen, London, UK. doi:10.5772/57268.

Gonçalves, G. C., Pereira, N. C. & Veit, M. T. 2016 Production of bio-oil and activated carbon from sugarcane bagasse and molasses. *Biomass and Bioenergy* **85**, 178–186. doi:10.1016/j.biombioe.2015.12.013.

Gonçalves Jr., A. C., Coelho, G. F., Schwantes, D., Rech, A. L., Campagnolo, M. A. & Miola Jr., A. 2016 Biosorption of Cu (II) and Zn (II) with acai endocarp *Euterpe oleracea* M. in contaminated aqueous solution. *Acta Scientiarum. Technology* **38**, 361–371. doi:10.4025/actascitechnol.v38i3.28294.

He, X., Che, R., Wang, Y., Li, Y., Wan, L. & Xiang, X. 2015 Core–nanoshell magnetic composite material for adsorption of Pb (II) in wastewater. *Journal of Environmental Chemical Engineering* **3**, 1720–1724. doi:10.1016/j.jece.2015.06.013.

Water Practice & Technology Vol 15 No 4
doi: 10.2166/wpt.2020.069

Hokkanen, S., Bhatnagar, A. & Sillanpää, M. 2016 A review on modification methods to cellulose-based adsorbents to improve adsorption capacity. *Water Research* **91**, 156–173. doi:10.1016/j.watres.2016.01.008.

Huang, L., Liu, L., Zhang, T., Zhao, D., Li, H., Kinney, P. L., Pitiranggon, M., Cillrud, S., Ma, L. Q., Navas-Acien, A., Bi, J. & Yan, N. 2019 An interventional study of rice for reducing cadmium exposure in a Chinese industrial town. *Environment International* **122**, 301–309. doi:10.1016/j.envint.2018.11.019.

IARC. International Agency For Research On Cancer 2018. Available from: https://monographs.iarc.fr/wp-content/uploads/2018/06/mono100C-8.pdf (accessed 12 July 2020).

Ibrahim, W. M., Hassan, A. F. & Azab, Y. A. 2016 Biosorption of toxic heavy metals from aqueous solution by *Ulva lactuca* activated carbon. *Egyptian Journal of Basic and Applied Sciences* **3**, 241–249. doi:10.1016/j.ejbas.2016.07.005.

IUPAC. International Union Of Pure And Applied Chemistry 1985 Reporting physisorption data for gas/solid systems with special reference to the determination of surface area and porosity. *Pure Applied Chemistry* **57**, 603–619.

Kan, Y., Yue, Q., Liu, S. & Gao, B. 2018 Effects of Cu and CuO on the preparation of activated carbon from waste circuit boards by H3PO4 activation. *Chemical Engineering Journal* **331**, 93–101. doi:10.1016/j.cej.2017.08.113.

Kawahigashi, F. 2012 *Aplicabilidade do pós-tratamento de lixiviados de aterro sanitário por adsorção em carvão ativado granular e avaliação ecotoxicológica*. *MSc. Thesis (MSc in Building and Sanitation Engineering)*, Universidade Estadual de Londrina, Londrina, Brazil.

Králik, M. 2014 Adsorption, chemisorption, and catalysis. *Chemical Papers* **68**(12). doi:10.2478/s11696-014-0624-9.

Kubier, A., Wilkin, R. T. & Pichler, T. 2019 Cadmium in soils and groundwater: a review. *Applied Geochemistry* **108**(104388). doi:10.1016/j.apgeochem.2019.104388.

Langmuir, I. 1918 The adsorption of gases on plane surfaces of glass, mica and platinum. *Journal of the American Chemical Society* **40**(9), 1361–1403. doi:10.1021/ja02242a004.

Lo, S. F., Wang, S. Y., Tsai, M. J. & Lin, L. D. 2012 Adsorption capacity and removal efficiency of heavy metal ions by Moso and Ma bamboo activated carbons. *Chemical Engineering Research and Design* **90**, 1397–1406. doi:10.1016/j.cherd.2011.11.020.

Mahmood, A. & Malik, R. N. 2014 Human health risk assessment of heavy metals via consumption of contaminated vegetables collected from different irrigation sources in Lahore, Pakistan. *Arabian Journal of Chemistry* **7**, 91–99. doi:10.1016/j.arabjc.2013.07.002.

Marcus, Y. 1993 Thermodynamics of solvation of ions. Part 6.–The standard partial molar volumes of aqueous ions at 298.15 K. *Journal of the Chemical Society, Faraday Transactions* **89**(4), 713–718. doi:10.1039/FT9938900713.

May, G. F., Davidson, A. & Monahov, V. 2018 Lead batteries for utility energy storage: a review. *Journal of Energy Storage* **15**, 145–157. doi:10.1016/j.est.2017.11.008.

Mimura, A. M. S., Vieira, T. V. A., Martelli, P. B. & Gorgulho, H. F. 2010 Aplicação da casca de arroz na adsorção dos íons Cu^{2+}, Al^{3+}, Ni^{3+} e Zn^{2+}. *Química Nova* **33**(6), 1279–1284. doi:10.1590/S0100-40422010000600012.

Nacke, H., Gonçalves Jr., A. C., Coelho, G. F., Schwantes, D., Campagnolo, M. A., Leismann, E. A. V., Conradi Jr., E. & Miola, A. J. 2017 Removal of Cd (II) from water using the waste of jatropha fruit (*Jatropha curcas* L.). *Applied Water Science* **7**, 3207–3222. doi 10.1007/s13201-016-0468-2.

Nascimento, R. F., Lima, A. C. A., Vidal, C. B., Melo, D. Q. & Raulino, G. S. C. R. 2014 *Adsorção: aspectos teóricos e aplicações ambientais. Org. Ivanaldo Maciel de Lima*. Imprensa Universitária, Fortaleza, p. 256. Available from: http://www.repositorio.ufc.br/bitstream/riufc/10267/1/2014_liv_rfdnascimento.pdf (accessed 12 July 2020).

Negara, D. N. K. P., Nindhia, T. G. T., Surata, W., Hidajat, F. & Sucipta, M. 2020 Textural characteristics of activated carbons derived from tabah bamboo manufactured by using H_3PO_4 chemical activation. *Materials Today: Proceedings* **22**(Part 2), 148–155. doi:10.1016/j.matpr.2019.08.030.

Nethaji, A., Sivasamy, A. & Mandal, A. B. 2013 Adsorption isotherms, kinetics and mechanism for the adsorption of cationic and anionic dyes onto carbonaceous particles prepared from Juglans regia shell biomass. *International Journal of Environmental Science and Technology* **10**(2). doi:10.1007/s13762-012-0112-0.

Nobrega, I. 2019 *57% of Cigarettes Sold in Brazil in 2019 are Illegal (Translated From Portuguese)*. Available from: https://www.poder360.com.br/brasil/57-dos-cigarros-vendidos-no-brasil-em-2019-sao-ilegais/ (accessed 12 July 2020).

Observatory of the National Policy on Tobacco Control. 2020 *Illegal Tobacco Market (Translated From Portuguese)*. Available from: https://www.inca.gov.br/en/node/1688 Last update: 02/20/2020. (accessed 12 July 2020).

Oginni, O., Singh, K., Oporto, G., Dawson-Andoh, B., Mcdonald, L. & Sabolsky, E. 2019 Effect of one-step and two-step H3PO4 activation on activated carbon characteristics. *Biosource Technology Reports* **8**, 100307. doi:10.1016/j.biteb.2019.100307.

Oliveira, L. S. & Franca, A. S. 2011 Conventional and non-conventional thermal processing for the production of activated carbons from agro-industrial wastes. *Activated Carbon: Classifications, Properties and Applications* **11**, 205–238.

Onorevoli, B., Maciel, G. P. S., Machado, M. E., Corbelini, V., Camarão, E. B. & Jacques, R. A. 2018 Characterization of feedstock and biochar from energetic tobacco seed waste pyrolysis and potential application of biochar as an adsorbent. *Journal of Environmental Chemical Engineering* **6**(1), 1279–1287. doi:10.1016/j.jece.2018.01.039.

Özer, E. T., Sarikaya, A. G. & Orman, B. 2016 Adsorption and removal of diethyl phthalate from aqueous media with poly(hydroxyethyl methacrylate) nanobeads. *Journal Desalination and Water Treatment* **57**. doi:10.1080/19443994.2016.1186568.

Peng, Y. & Wu, S. 2010 The structural and thermal characteristics of wheat straw hemicellulose. *Journal of Analytical and Applied Pyrolysis* **88**(2). doi:10.1016/j.jaap.2010.03.006.

Water Practice & Technology Vol 15 No 4
doi: 10.2166/wpt.2020.069

Penha, R. S., Santos, C. C., Cardoso, J. J., Silva, H. A., Santana, S. A. & Bezerra, C. W. B. 2016 Chemically treated rice husk as low cost adsorbent for metal ions uptake (CO^{2+} and Ni^{2+}). *Revista Virtual de Química* **8**, 588–604. doi:10.5935/1984-6835.20160045.

Pongener, C., Bhomich, P. C., Supong, A., Baruah, M., Sinha, U. B. & Sinha, D. 2018 Adsorption of fluoride onto activated carbon synthesized from Manihot esculenta biomass – equilibrium, kinetic and thermodynamic studies. *Journal of Environmental Chemical Engineering* **6**(2), 2382–2389. doi:10.1016/j.jece.2018.02.045.

Quesada-Plata, F., Ruiz-Rosas, R., Morallón, E. & Cazorla-Amoróz, D. 2016 Activated carbons prepared through H_3PO_4-assisted hydrothermal carbonisation from biomass wastes: porous texture and electrochemical performance. *ChemPlusChem* **81**(12), 1349–1359. doi:10.1002/cplu.201600412.

Reyes-Hinojosa, D., Lozada-Pérez, C. A., Cuevas, Y. Z., Lópes-Reyes, A., Martínez-Nava, G., Fernández-Torres, J., Olivos-Meza, A., Landa-Solis, C., Gutiérrez-Ruiz, M. C., Castillo, R. D. & Martínez-Flores, K. 2019 Toxicity of cadmium in musculoskeletal diseases. *Environemental Toxicology and Pharmacology* **72**, 103219. doi:10.1016/j.etap.2019.103219.

Rocha, A. & Trujillo, K. A. 2019 Neurotoxicity of low-level lead exposure: history, mechanisms of action, and behavioral effects in humans and preclinical models. *NeuroToxicology* **73**, 58–80. doi:10.1016/j.neuro.2019.02.021.

Rodriguez, M. H., Yperman, J., Carleer, R., Maggen, J., Dadi, D., Gryglewicz, G. & Calvis, A. O. 2018 Adsorption of Ni (II) on spent coffee and coffee husk based activated carbon. *Journal of Environmental Chemical Engineering* **6**, 1161–1170. doi:10.3390/environments7040024.

Sardella, F., Gimenez, M., Navas, C., Morandi, C., Deiana, C. & Sapag, K. 2015 Conversion of viticultural industry wastes into activated carbons for removal of lead and cadmium. *Journal of Environmental Chemical Engineering* **3**, 253–260. doi:10.1016/j.jece.2014.06.026.

Schiller, A. P., Ferronato, M. C., Schwantes, D., Gonçalves, A. C., Barili, D. J. & Manfrin, J. 2019 Influence of hydrological flows from tropical watersheds on the dynamics of Cu and Zn in sediments. *Environmental Monitoring and Assessment* **191**, 86. doi:10.1007/s10661-019-7193-x.

Schiller, A. P., Gonçalves Jr., A. C., Braccini, A. L., Schwantes, D., Campagnolo, M. A., Conradi Jr., E. & Zimmermann, J. 2020 Potential of agricultural and agroindustrial wastes as adsorbent materials of toxic heavy metals: a review. *Desalination and Water Treatment* **187**, 203–218. doi:10.5004/dwt.2020.25094.

Schiller, A. P., Schwantes, D., Gonçalves Jr., A. C., Manfrin, J., Campagnolo, M. A., Dullius, T., Aleixo, V., Richart, A. & Tejada, E. S. 2018 *Spirodela polyrhiza* na fitorremediação e pós-tratamento de efluente doméstico. *Revista de Estudos Ambientais* **19**, 17–30. doi: 10.7867/1983-1501.2017v19n2p17-30.

Schwantes, D., Gonçalves, A. C., Campagnolo, M. A., Tarley, C. R. T., Dragunski, D. C., Manfrin, J. & Schiller, A. D. P. 2018a Use of co-products from the processing of cassava for the development of adsorbent materials aiming metal removal. In: *Cassava* (Waisundara, V., ed.). InTech, p. 265-290. doi:10.5772/intechopen.71048.

Schwantes, D., Gonçalves Jr., A. C., Campagnolo, M. A., Tarley, C. R. T., Dragunski, D. C., De Varennes, A., Silva, A. K. D. S. & Conradi Jr., E. 2018b Chemical modifications on pinus bark for adsorption of toxic metals. *Journal of Environmental Chemical Engineering* **6**, 1271–1278. doi:10.1016/j.jece.2018.01.044.

Shamsudin, M. S., Azha, S. F., Shahadat, M. & Ismail, S. 2019 Cellulose/bentonite-zeolite composite adsorbent material coating for treatment of N-based antiseptic cationic dye from water. *Journal of Water Process Engineering* **29**, 100764. doi:10.1016/j.jwpe.2019.02.004.

Silverstein, R. M., Webster, F. X., Kiemle, D. J. & Bryce, D. L. 2014 *Spectrometric Identification of Organic Compounds*, 8th edn. Wiley, Hoboken, NJ, p. 464.

Sips, R. 1948 Combined form of Langmuir and Freundlich equations. *The Journal of Chemical Physics* **16**, 490–495.

Tagliaferro, G., Pereira, P., Rodrigues, L. & Silva, M. 2011 Cadmium, lead and silver adsorption in hydrous niobium oxide prepared by homogeneous solution method. *Química Nova* **4**, 101–105. doi:10.1590/S0100-40422011000100020.

Temkin, M. I. & Pyzhev, V. 1940 Kinetics of ammonia synthesis on promoted iron catalyst. *Acta Physiochim* URSS **12**, 327–356.

Thommes, M., Kaneko, K., Neimark, A. V., Olivier, J. P., Rodriguez-Reinoso, F., Rouquerol, J. & Sing, K. S. W. 2015 Physisorption of gases, with special reference to the evaluation of surface area and pore size distribution (IUPAC Technical Report). *Pure and Applied Chemistry* **87**(9-10), 1051–1069. doi:10.1515/pac-2014-1117.

Torkashvand, J., Farzadkia, M., Sobji, H. R. & Esrafili, A. 2020 Littered cigarette butt as a well-known hazardous waste: a comprehensive systematic review. *Journal of Hazardous Materials* **383**, 121242. doi:10.1016/j.jhazmat.2019.121242.

Tural, B., Ertas, E. & Tural, S. 2016 Removal of phenolic pollutants from aqueous solutions by a simple magnetic separation. *Desalination and Water Treatment* **57**, 26153–26164. doi:10.1080/19443994.2016.1162202.

UN. United Nations 2015 *Conheça os 17 objetivos da ONU para o desenvolvimento sustentável*. Available from: https://nacoesunidas.org/conheca-os-novos-17-objetivos-de-desenvolvimento-sustentavel-da-onu/ (accessed 11 November 2019).

Welz, B. & Sperling, M. 2008 *Atomic Absorption Spectrometry*, 3rd edn. Wiley-VCH, Weinheim, Germany.

WHO. World Health Organization 2011a *Cadmium in Drinking-Water – Background Document for Development of WHO Guidelines for Drinking-Water Quality*. WHO, Geneva, Switzerland. Available from: https://www.who.int/water_sanitation_health/dwq/chemicals/cadmium.pdf (accessed 8 July 2020).

WHO. World health organization 2011b *Lead in Drinking-Water – Background Document for Development of WHO Guidelines for Drinking-Water Quality*. WHO, Geneva, Switzerland. Available from: https://www.who.int/water_sanitation_health/dwq/chemicals/lead.pdf (accessed 8 July 2020).

Water Practice & Technology Vol 15 No 4
doi: 10.2166/wpt.2020.069

Xing, X., Jiang, W., Li, S., Zhang, X. & Wang, W. 2019 Preparation and analysis of straw activated carbon synergetic catalyzed by zncl$_2$-H_3PO_4 through hydrothermal carbonization combined with ultrasonic assisted immersion pyrolysis. *Waste Management* **89**, 64–72. doi:10.1016/j.wasman.2019.04.002.

Zein, R., Suhaili, R., Earnestly, F. & Indrawati, E. M. 2010 Removal of Pb(II), Cd(II) and Co(II) from aqueous solution using *Garcinia mangostana* L. fruit shell. *Journal of Hazardous Materials* **181**, 52–56. doi:10.1016/j.jhazmat.2010.04.076.

Zulfiqar, U., Farooq, M., Hussain, S., Maqsood, M., Hussain, M., Ishfaq, M., Ahmad, M. & Anjum, M. Z. 2019 Lead toxicity in plants: impacts and remediation. *Journal of Environmental Management* **250**, 109557. doi:10.1016/j.jenvman.2019.109557.